

# Cosmic ray topography

Matthew Bressler, Lydia Goodwin, and Abaz Kryemadhi<sup>a)</sup>

*Department of Math, Physics, and Statistics, Messiah College, Mechanicsburg, Pennsylvania 17055*

(Received 21 July 2016; accepted 13 July 2017)

Cosmic ray muons are produced when high energy particles interact with nuclei in Earth's atmosphere. Muons make up the majority of charged particles that reach sea level and are the only particles (apart from neutrinos) that can penetrate to significant depths underground. The muon flux underground decreases approximately exponentially as a function of depth. We use a cosmic ray detector developed by the QuarkNet Program at Fermi National Laboratory to map the topography of the mountain above an abandoned Pennsylvania Turnpike tunnel by analyzing muon flux at different rock overburdens. Cosmic ray muons have been used in this capacity before to search for hidden chambers in pyramids and for mapping volcanoes. This study provides a unique field experience to learn about particle physics and particle detectors, which could be of interest to students and teachers in physics. © 2017 American Association of Physics Teachers.

[<http://dx.doi.org/10.1119/1.4996874>]

## I. INTRODUCTION

Primary cosmic rays are produced from the sun, supernovae, black holes, and active galactic nuclei and include protons, electrons, and nuclei. When these primary particles encounter Earth's atmosphere, they interact with nuclei in the atmosphere and secondary cosmic rays are produced in the collisions.<sup>1</sup> Cosmic ray muons are produced in these reactions at (typical) heights of 15 km and have long decay lengths owing to time dilation. They are the most abundant charged particles at Earth's surface with a flux of one muon per cm<sup>2</sup> per minute.<sup>1,2</sup> The flux decreases exponentially with depth as muons travel underground, which is why experiments such as the Super Cryogenic Dark Matter Search Experiment operate deep underground where this unwanted cosmogenic contribution is reduced to essentially zero.<sup>3</sup> Cosmic rays have been used for determining the amount of rock overburden on tunnels, imaging of volcanoes, and searching for hidden chambers inside pyramids.<sup>4-7</sup> In this study, we mapped the topography of the mountain above the Rays Hill tunnel by measuring the cosmic ray flux inside the tunnel. Rays Hill is one of three original Pennsylvania Turnpike tunnels that were abandoned<sup>8</sup> in 1968. The tunnel is located between Bedford and Fulton counties in southern Pennsylvania and has a length of 1077 m (3550 ft). Figure 1 shows a topographic map of the tunnel and the surrounding area.

A bonus element of this study is the availability of cosmic ray detectors developed for outreach and research that are located in many high schools, colleges, and universities. This makes it convenient to repeat the experiment in different locations without the extra cost of purchasing equipment. For a non-exhaustive review of these experiments see Ref. 10 and for a recent classroom use of cosmic ray detectors in the undergraduate curriculum see Refs. 11–15.

## II. EXPERIMENT

The cosmic ray detector we used was developed for the QuarkNet program at Fermi National Accelerator Laboratory.<sup>16</sup> The schematic of the detector is shown in Fig. 2. The plastic scintillators convert the muon ionization energy losses to electrical pulses, and the data acquisition

board (DAQ) processes these pulses and sends them to a computer. For further information about this detector or particle detectors generally, see Refs. 16 and 17. The area of our scintillators is  $0.25 \text{ m} \times 0.25 \text{ m} = 0.0625 \text{ m}^2$  and the distance between the two scintillators is fixed at  $d = 0.25 \text{ m}$ . The tunnel has no electricity so a portable power pack was used to provide power for the detector and laptop computer. All the detector components were carried in a backpack and the detector was assembled outside the tunnel as shown in Fig. 3. When everything was assembled, we entered through the western side of the tunnel and had enough power to collect 25 data points at 10 min intervals, which was sufficient for our purposes. In this configuration, we obtained flux data every 150 feet of horizontal distance into the tunnel.

## III. RESULTS

A cosmic ray muon is counted if both plastic scintillators record a pulse above a certain threshold. The threshold voltage was fixed at 300 mV for each detector, which corresponds to a voltage of 30 mV before amplifier and after the photomultiplier tube (PMT). We assessed the uniformity and detection efficiency of our scintillators for cosmic ray muons by using a Geant4 Monte Carlo simulation, which simulates the energy losses of particles in the scintillator and the generation of optical photons and their passage through scintillator material and PMT.<sup>18</sup> We provided the detector geometry and different properties for the scintillator and the PMT used, and found the average number of photoelectrons in the PMT. We varied the location of the muon incidence within the scintillator and observed that the number of photoelectrons varied from 50 photoelectrons farthest away from the PMT to 400 photoelectrons closest to the PMT. We then calculated the voltage output for one photoelectron. Given a gain of  $G = 3 \times 10^6$ , time width of  $\approx 7.5 \text{ ns}$ , and output impedance of  $R = 50 \Omega$ , we obtained<sup>19,20</sup>  $V = q/tR \approx eGR/t \approx 3.0 \text{ mV}$ . With a threshold of 30 mV at the PMT level, we are 100% efficient ( $\epsilon = 1$ ) anywhere in the scintillator for the number of photoelectrons reported from Geant4 simulation.

Another consideration is the accidental rate in the muon flux. With a single rate of  $\approx 40 \text{ Hz}$  and a coincidence window of 100 ns, the accidental rate is  $\approx 0.0002$  muons per second. Thus, the accidental rate is negligible across all rates we have in our data.



Fig. 1. A map of Rays Hill Tunnel from Google maps.

The vertical intensity

$$I_p = \frac{\text{Flux}}{\epsilon A \Delta\Omega} \quad (1)$$

is commonly quoted in the literature, where  $A$  is the area of one scintillator counter and  $\Delta\Omega$  is the solid angle subtended by the top scintillator as viewed from a small area of the bottom scintillator.<sup>1</sup> The solid angle is crudely found to be  $\Delta\Omega \approx wl/d^2 \approx 1$  sr for our detector geometry. The calculated vertical intensity is  $I_p \approx 70 \text{ m}^{-2} \text{ sr}^{-1} \text{ s}^{-1}$  given our measured flux of 5 muons per second outside the tunnel, which agrees with other surface level muon measurements in the literature.<sup>1,9</sup> The vertical intensity measurement is an important benchmark to ensure proper working of our detector. The rate data collected are shown in Table I.

The area and solid angle of our detector are kept constant through all the measurements so we factored them out and used the rate directly to calculate the height. For the intensity versus depth curve, we used an empirical expression developed by Barbouti,<sup>21</sup> which is valid across the ranges of overburden we have. This formula is given by

$$I_v(h) = \frac{K e^{-\beta h}}{(h^\alpha + a)(h + H)} \text{ particles cm}^{-2} \text{ s}^{-1} \text{ sr}^{-1}, \quad (2)$$

where  $\alpha = 1.68$ ,  $K = 270.7 \text{ hg/cm}^2$ ,  $a = 75$ ,  $H = 200 \text{ hg/cm}^2$ ,  $\beta = 5.5 \times 10^{-4} \text{ hg}^{-1} \text{ cm}^2$ , and 1 hectogram (hg) = 0.1 kg. The measured rate was used in conjunction with Eq. (2) to determine the overburden depth.

Figure 4 shows the actual topography<sup>22</sup> and the one obtained by cosmic ray flux measurements before we applied the solid angle correction. There are differences between the actual and the measured topography, particularly around the

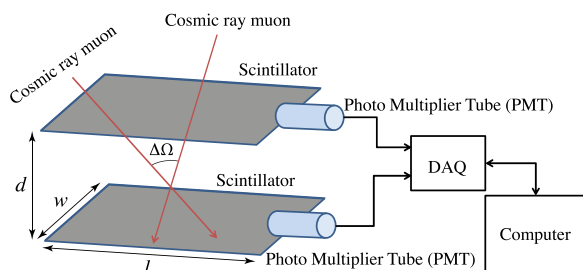


Fig. 2. Schematic of the cosmic ray detector.

peak. In order to understand the disagreement, we used the MUSIC Simulation Code,<sup>23</sup> where we generated muons at the surface level according to the known energy and angular distribution as specified in Ref. 1, and provided the two dimensional shape of the mountain. The code propagates cosmic rays through rock by simulating their energy losses, multiple Coulomb Scattering, and other processes. The detector geometry and the number of events were the same as in the experiment. Figure 4 shows that the simulation follows the experimental data more closely than the actual topography, hinting that the solid angle is the source of the discrepancy. The error bars both in data and simulation are statistical only.

We examined the possibility of improving our measurements by correcting for the solid angle. The sketch in Fig. 5 aids us in the following discussion. The solid angle is the same for different locations ( $x_1$ ,  $x_2$ , and  $x_3$ ) in the tunnel, as represented by the zenith angle variation  $\Delta\theta$ , but the corresponding horizontal resolutions ( $\sigma_1$ ,  $\sigma_2$ , and  $\sigma_3$ ) are different because of the different heights ( $z_1$ ,  $z_2$ , and  $z_3$ ). The resolution gets worse with increased height, which is consistent with the observed larger discrepancies around the peak, as seen in Fig. 4. A detector located at point  $x_3$  accepts events within the  $\Delta\theta$  zenith angle or within  $x_3 \pm \sigma_3$ , consequently there is a smearing effect where measurements at one particular location are correlated with measurements at different locations. The unfolding techniques are used to extract true distributions from measured ones.<sup>24,25</sup>

The folding and (inverse) unfolding processes are described by the Fredholm integral of the first kind. The integral for folding (convolution) is given by<sup>25</sup>



Fig. 3. Setting up the detector just outside of the tunnel.

Table I. Muon rate data.

Distance into tunnel (ft)	Muon Rate (particles/s)
0	5
150	0.39
300	0.2
450	0.12
600	0.06
750	0.07
900	0.05
1050	0.04
1200	0.03
1350	0.03
1500	0.02
1650	0.02
1800	0.02
1950	0.02
2100	0.03
2250	0.02
2400	0.03
2550	0.05
2700	0.07
2850	0.06
3000	0.1
3150	0.15
3300	0.27
3450	3.3
3600	5.95

$$D_m(x) = \int K(\sigma, u - x) D_p(u) du, \quad (3)$$

where  $K(\sigma, u - x) = (\sigma\sqrt{\pi})^{-1} \exp[-(u - x)^2/\sigma^2]$  is a Gaussian kernel,  $D_m(x)$  is the measured value at  $x$ , and  $D_p(u)$  is the true distribution at  $u$ . The integral for unfolding (de-convolution) is given by<sup>25</sup>

$$D_p(x) = \int K^{-1}(\sigma, u - x) D_m(u) du. \quad (4)$$

Here,  $K^{-1}(\sigma, u - x)$  is the inverse Gaussian kernel, which in Ref. 25 is given by

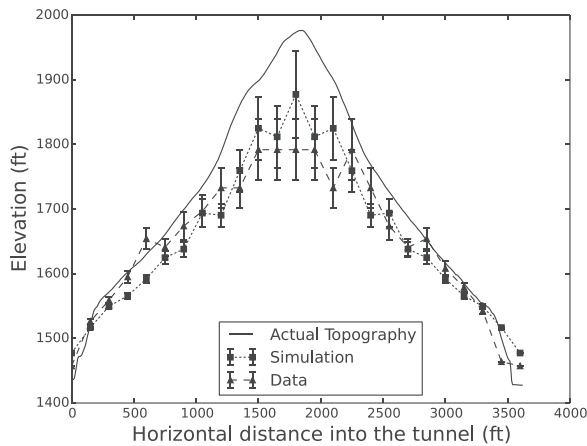


Fig. 4. The actual topography (solid), along with the topography obtained using cosmic ray muon data (square-dashed) and simulation (triangle-dotted) before applying solid angle correction.

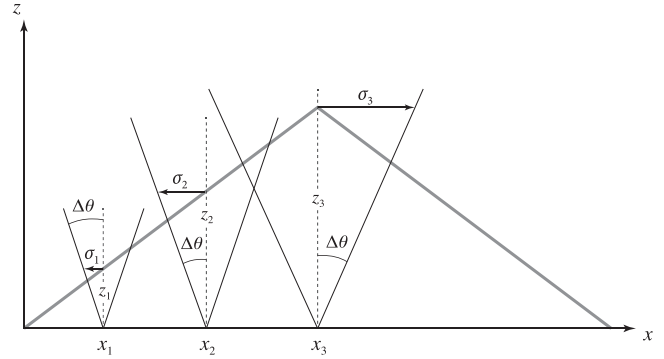


Fig. 5. The geometry of solid angle for different heights.

$$K^{-1}(\sigma, u - x) = \sum_{n=0}^{\infty} c_n(\sigma) H_{2n} \left( \frac{u - x}{\sigma} \right) K(\sigma, u - x), \quad (5)$$

where  $H_{2n}(\xi)$  are the Hermite Polynomials,  $c_n(\sigma) = (-1)^n \sigma^{2n}/(2^n n!)$  are expansion coefficients, and  $K(\sigma, u - x)$  is the Gaussian convolution function. An expansion in terms of Hermite Polynomials is very useful because of the orthogonality condition  $\int e^{-x^2} H_n(x) H_m(x) dx \propto \delta_{nm}$ . The Gaussian smearing is localized in the vicinity of the point in consideration with a range of  $\pm\sigma$ . It is reasonable to assume a piecewise linear mountain profile within this range, hence  $D_m(u)$  can be expressed as a linear combination  $\alpha H_0(u) + \beta H_1(u)$ . Given the orthogonality condition, the only non-vanishing contribution in the inverse Gaussian kernel is from the  $H_0[(x - u)/\sigma] K(\sigma, x - u)$  term, which is just the Gaussian function since  $H_0[(x - u)/\sigma] = 1$ .

A Gaussian function was therefore used to unfold the true heights  $h_i$  from measured heights  $h_m$  in light of the above discussion, giving

$$h_i(i) = \frac{\sum_j e^{-[x(i) - x(j)]^2/\sigma^2(i)} h_m(j)}{\sum_j e^{-[x(i) - x(j)]^2/\sigma^2(i)}}, \quad (6)$$

where  $\sigma(i)$  is the resolution at position  $x(i)$ , given by  $\sigma(i) \approx \Delta\theta z(i) = \Delta\theta h_m(i)$ . The zenith angle variation  $\Delta\theta$  was extracted from a least squares optimization by comparing the fitted data with the actual profile, and was found to be 0.37 rad. The resolutions are, for instance, 0.37 m at a height of 1 m and 60 m at a height of 160 m. We draw the attention to the fact that in the absence of the solid angle corrections these resolutions determine the minimum size of a cavity that can be resolved as a function of height of the cavity.

Figure 6 shows the topography after we applied the unfolding to both data and simulated events. There is now good agreement between the actual topography and the data. The experimental results are closer to the actual topography than the simulation results, mainly because the simulation does not account for non-homogeneities of the rock and is limited to two dimensions.

The experimental measurements could be made more precise by increasing the collection time and decreasing the solid angle. However, we needed to complete the data collection within one day for it to be a practical field trip experience. A smaller solid angle makes unfolding corrections smaller. In the simulation, we examined a scenario where the solid angle decreased by approximately a factor of ten (increase distance  $d$  by a factor of 3.3). The reduction of the solid angle yields a reduction in

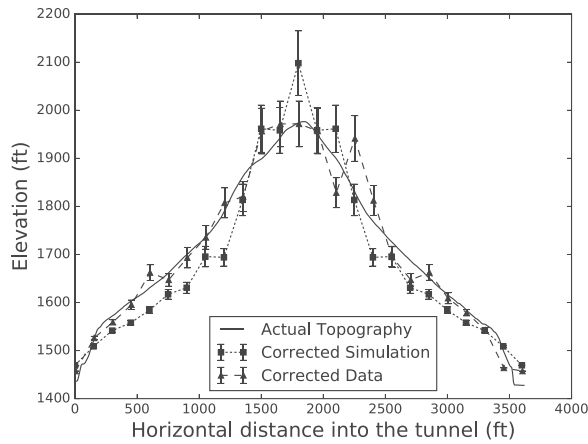


Fig. 6. The topography after applying solid angle correction.

muon rate by a factor of  $\sim 37$  due to the much smaller acceptance of our telescope. At the same time, we increased the overall counts in the simulation by a factor of 10, resulting in a time interval that is  $37 \times 10 = 370$  times longer compared to the actual experiment performed. In this scenario, one would need about two-and-a-half days to collect a single data point, or about two months to complete the entire 25-data-point experiment. When collecting data for such long times, one should consider the environmental effects such as pressure variation in cosmic ray flux, which were negligible in our short time window.

#### IV. CONCLUSION

We determined the topography of the mountain above the Rays Hill tunnel using cosmic ray muons. We found that the solid angle was the main limiting factor for our measurements, but were able to overcome this limitation by applying an unfolding technique. The topography obtained from cosmic ray measurements after correcting for the solid angle agrees remarkably well with the actual topography. Any small disagreement is ascribed to multiple Coulomb Scattering and non-homogeneity of the rock overburden. The measurement presented in this paper can be used to look for rock overburdens in tunnels or large cavities in caves while providing an excellent field experience for high school or undergraduate students, allowing them to learn about particle detectors and particle physics.

#### ACKNOWLEDGMENTS

The authors thank the QuarkNet Program at Fermi National Accelerator Laboratory for providing the detector, Messiah College for support of the project, and the anonymous reviewers who helped make this study much more comprehensive.

<sup>a)</sup>Electronic mail: akryemadhi@messiah.edu

- <sup>1</sup>K. A. Olive *et al.*, “Cosmic ray section of particle data group,” *Chin. Phys. C*, **38**, 090001 (2014).
- <sup>2</sup>Claus Grupen, *Astroparticle Physics* (Springer, Berlin/Heidelberg, Germany, 2005).
- <sup>3</sup>The Super Cryogenic Dark Matter Search (SCDMs) collaboration website can be found at <http://cdms.berkeley.edu/experiment.html>.
- <sup>4</sup>E. P. George, “Cosmic rays measure overburden of tunnel,” *Commonw. Eng.* **1955**, 455–457 (1955).
- <sup>5</sup>Ch. J. Rhodes, “Muon tomography: Looking inside dangerous places,” *Sci. Prog.* **98**(3), 291–299 (2015).
- <sup>6</sup>Hiroyuki K. M. Tanaka, “Muographic mapping of the subsurface density structures in Miura, Boso and Izu peninsulas, Japan,” *Sci Rep.* **5**, 8305–8315 (2015).
- <sup>7</sup>L. W. Alvarez *et al.*, “Search for hidden chambers in the pyramids,” *Science* **167**, 832–839 (1970).
- <sup>8</sup>More information on Rays Hill tunnel can be found at [https://en.wikipedia.org/wiki/Rays\\_Hill\\_Tunnel](https://en.wikipedia.org/wiki/Rays_Hill_Tunnel).
- <sup>9</sup>L. N. Bogdanova, M. G. Gavrilo, V. N. Kornoukhov, and A. S. Starostin, “Cosmic muon flux at shallow depths underground,” *Phys. At. Nucl.* **69**(8), 1293–1298 (2006).
- <sup>10</sup>R. A. Soluk and ALTA Collaboration, “Educational cosmic ray arrays,” *AIP Conf. Proc.* **828**, 271–276 (2006).
- <sup>11</sup>R. Guntera, G. Spiczak, and J. Madsen, “Cosmic collaboration in an undergraduate astrophysics laboratory,” *Am. J. Phys.* **78**, 1035–1047 (2010).
- <sup>12</sup>B. Brau, C. May, R. Ormond, and J. Essick, “Determining the muon mass in an instructional laboratory,” *Am. J. Phys.* **78**, 64–70 (2010).
- <sup>13</sup>Th. Coana, T. Liub, and J. Ye, “A compact apparatus for muon lifetime measurement and time dilation demonstration in the undergraduate laboratory,” *Am. J. Phys.* **74**, 161–164 (2006).
- <sup>14</sup>D. P. Jackson and M. T. Welker, “Measuring and modeling cosmic ray showers with an MBL system: An undergraduate project,” *Am. J. Phys.* **69**, 896–900 (2001).
- <sup>15</sup>N. Easwar and D. A. MacIntire, “Study of the effect of relativistic time dilation on cosmic ray muon flux An undergraduate modern physics experiment,” *Am. J. Phys.* **59**, 589–592 (1991).
- <sup>16</sup>S. Hansen *et al.*, “Low-cost data acquisition card for school-network cosmic ray detectors,” *IEEE Trans. Nucl. Sci.* **51**(3), 926–930 (2004); website for quarknet cosmic ray detector activities: <http://quarknet.fnal.gov/>.
- <sup>17</sup>Abaz Kryemadhi and Kyler Chrestay, “Gamma ray spectroscopy with a silicon photomultiplier and a LYSO crystal,” *Am. J. Phys.* **83**, 378–381 (2015).
- <sup>18</sup>S. Agostinelli *et al.*, “Geant4 a simulation toolkit,” *NIM. A* **506**(3), 250–303 (2003).
- <sup>19</sup>Private Communication with [www.sens-tech.com](http://www.sens-tech.com).
- <sup>20</sup>G. F. Knoll, *Radiation Detection and Measurement*, 4th ed. (Wiley, New York, NY, 2010).
- <sup>21</sup>A. I. Barbouti and B. C. Rastin, “A study of the absolute intensity of muons at sea level and under various thicknesses of absorber,” *J. Phys. G: Nucl. Phys.* **9**, 1577–1595 (1983).
- <sup>22</sup>The actual topography data was obtained from <http://www.geocontext.org/publ/2010/04/profiler/en/>.
- <sup>23</sup>V. A. Kudryavtsev, “Muon simulation codes MUSIC and MUSUN for underground physics,” *Comput. Phys. Commun.* **180**, 339–346 (2009); V. A. Kudryavtsev, E. V. Korolkova, and N. J. C. Spooner, “Narrow muon bundles from muon pair production in rock,” *Phys. Lett. B* **471**, 251–256 (1999); P. Antonioli, C. Ghetti, E. V. Korolkova, V. A. Kudryavtsev, and G. Sartorelli, “A three-dimensional code for muon propagation through the rock: MUSIC,” *Astropart. Phys.* **7**, 357–268 (1997).
- <sup>24</sup>G. Cowan, “A survey of unfolding methods for particle physics,” *Conf. Proc. C0203181*, 248–257 (2002).
- <sup>25</sup>W. Ulmer and W. Kaissl, “The inverse problem of a Gaussian convolution and its application to the finite size of the measurement chambers/detectors in photon and proton dosimetry,” *Phys. Med. Biol.* **48**, 707–727 (2003).